Nonlinear optical and antimicrobial activity of N-acyl glycine derivatives

Nour El Houda Nourai, Fatiha Sebih, Djebar Hadji, Fatima Zohra Allal, Soulef Dib, Nadia Kambouche, Valérie Rolland, Salima Bellahouel-Benzine

Journal of Molecular Liquids 398 (2024) 124260

Contents lists available at ScienceDirect

Journal of Molecular Liquids

journal homepage: www.elsevier.com/locate/molliq

Nonlinear optical and antimicrobial activity of N-acyl glycine derivatives

Nour El Houda Nourai [a], Fatiha Sebih [a,b], Djebar Hadji [c,d,*], Fatima Zohra Allal [a], Soulef Dib [e], Nadia Kambouche [a], Valérie Rolland [f], Salima Bellahouel-Benzine [a]

[a] Laboratoire de Synthèse Organique Appliquée (LSOA), Faculté des Sciences Exactes & Appliquées, Université Oran1, BP 1524 El M'Naouer, 31000 Oran, Algeria
[b] Department of Chemical Engineering, Faculty of Chemistry, University of Sciences and Technology Mohamed Boudiaf, BP 1505, El-Mnaouer, 31000, Oran, Algeria
[c] Modeling and Calculation Methods Laboratory, University of Saida – Dr. Moulay Tahar, Saïda, Algeria
[d] Department of Chemistry, Faculty of Sciences, University of Saida – Dr. Moulay Tahar, 20000 Saida, Algeria
[e] Laboratoire de Biologie des Microorganismes et Biotechnologie (LBMB), Faculté des Sciences de la Nature et de la Vie, Université Oran1, BP 1524 El M'Naouer, 31000 Oran, Algeria
[f] Institut des Biomolécules Max Mousseron, UMR5247 CNRS, Pôle Chimie Balard, Montpellier cedex5, France

ARTICLE INFO

Keywords:
Glycine
Lipoaminoacids
Nonlinear optic
Antimicrobial

ABSTRACT

The current paper provides a theoretical and experimental coupled study of synthesized N–octanoyl glycine and N–oleoyl glycine. The derivatives were characterized using nuclear magnetic resonance (^{1}H and ^{13}C NMR), liquid chromatography–mass spectrometry (LC-MS), Fourier–transform infrared (FT-IR), and ultraviolet–visible (UV–Vis) spectroscopy. The resulting N-acyl glycines were assessed for their *in vitro* antimicrobial activity. The experimental investigation is supported by a linear and nonlinear optical study based on DFT levels and shows that our glycine analogues get moderate hyperpolarizability (β). The β results of these glycines are of moderate amplitude, like those of amino acids. For this, several procedures have been discussed for achieving these β values.

1. Introduction

The chemistry of lipoaminoacid derivatives has undergone spectacular development in recent years at both experimental and theoretical levels. Lipoamino acids, also named N-acyl amino acids which are fatty acids conjugated to amino acids such as alanine and glycine [1]. Up to now, the literature describes various methods for producing amino acids [2–4], and the predominant method employed in industry for producing those surfactants is based on applying the Schotten-Baumann chemical and unselective reaction [3]. They are widely distributed in microorganisms, highly biocompatible and have minimal toxicity. Lipoamino acids have attracted much attention due to their potential use in biology [4]. Due to their structural resemblance to endocannabinoids, an endogenous signaling system involved in metabolism, cell proliferation, hunger, and neuro–modulatory effects, they have been discovered in mammalian species and have sparked renewed scientific interest [5]. Numerous biological processes [6], including bone mass and remodeling [7], anti-inflammatory properties [8], inhibition of cell proliferation, calcium ion mobilization [9], and brain protection, have been linked to lipoamino acids [10]. N-acyl amino acids as part of a family of bioactive lipids have exerted various roles in the construction of newer entities with better therapeutic effects and pharmacological profiles such as antihypertensive [11], anti-leishmanial [12], neuromodulators [13], anti-Parkinson [14], biostatic additives [15], antiproliferative [16], mucolytic [17], anticancer [18], antiulcer [19], enzyme inhibitors [5], analgesic [20], antifungal [21], antidepressant, and monoamine oxidase inhibitory activities [22]. Furthermore, a considerable number of these functional surface–active molecules spread throughout the literature, like softeners in soap manufacturing detergents and wetting agents. In addition, N-acyl amino acid surfactants derived from different vegetable oils, such as castor and cottonseed oil, have significantly influenced the interfacial properties [23]. Renewable amino acid–based surfactants can be identified as cleaning agents, and we noticed a terrible rise in their use during the coronavirus pandemic. These surfactants played a remarkable role in reducing the occurrence of infections and health risks. Natural biological fatty acids have an antibacterial impact on many bacteria [24]. Additionally, it has been claimed that fatty acids have broad–spectrum antibacterial effects with potencies on par with some naturally occurring antimicrobial peptides [25]. Long–chain unsaturated fatty acids are said to be more potent in general than saturated

* Corresponding author.
E-mail address: hadji120780@yahoo.fr (D. Hadji).

https://doi.org/10.1016/j.molliq.2024.124260
Received 24 November 2023; Received in revised form 29 January 2024; Accepted 11 February 2024
Available online 20 February 2024

fatty acids with the same chain length. Furthermore, a considerable number of those derivatives versus conventional fatty acids spread throughout potent thermogenic uncouplers in cells and mitochondria [26]. This efficiency was confirmed by examining the affinity of arachidonate vs N-arachidonoyl-glycine and oleate vs N–oleoyl–leucine in cells and mitochondria. Over the past few years, a substantial amount of work has gone into investigating N-acyl amino acids as a model protoamphiphilic system and outlining their interest in generating robust [27]. Acylated amino acids have been widely used as an efficient amino acid ligand–assisted Pd–catalyzed C–H activation of tethered arenes [28]. During a study on recently synthesized N-acyl sarcosines tested for corrosion protection by polarization and weight loss, Kaskah *et al.* [29] indicate that compounds present variations on the sarcosine carbon chain and are tested in 0.1 M NaCl as a protective barrier for low–carbon steel in salt water. These substances acting as mixed-type inhibitors with beneficial electronic properties have been vigorously explored in recent years [30]. In the contribution of Günay *et al.* [30], the authors have investigated the NLO behavior by the determination of the dipole moment, polarizability, and first-order hyperpolarizability of the N-acetyl-DL-methionine which is a derivative of the DL-methionine. The results showed that the hyperpolarizability values for this similar compound are higher than the urea and *para*-nitroaniline (*p*NA), which are well-known prototypical NLO materials. They highlighted frontier molecular and neighboring orbitals using the DFT methods with the 6–311 + G(d,p) basis set. The HOMO-LUMO energy gap results reveal that this molecule has the highest kinetic stability. Moreover, Farhan and co-workers [31] have performed DFT calculations to calculate various physicochemical descriptors of two similar fatty amides: hydroxamic fatty acids and fatty hydrazide hydrate. The authors showed that the ability of these chemicals to receive electrons is a prerequisite for antibacterial activity. In this study [31], the antibacterial properties occurred at regions with molecules having the highest softness and lowest hardness. Soft molecules are more readily available for the show features because they have a lower energy gap than complex molecules. In the same context, another study [32] shows the importance of the amide bonds contained in our Lipoaminoacids for designing new NLO materials. In addition, N-acyl amino acids have been used as ligands [16] to synthesize europium amino acid complexes (Eu $[CH_3(CH_2CH_2)_nCONHCH(CH_3)COO]_3$, which had good absorption capacity in the range of 200–300 nm. Other Studies [33,34] show that the formation of oligomers containing these units might achieve very large β responses for similar N-acyl glycine derivatives, which get moderate hyperpolarizability. This further corroborates that these materials possess the required characteristics for NLO applications. The optical and nonlinear optical activity of amino acids [35,36] and organic compounds has been shown in several studies [37–47]. This work aims to synthesize, characterize, test invitro antimicrobial activity, and analyze the polarizability and first-order hyperpolarizability of two lipoamino acids, which should be biodegradable, non-toxic, and inexpensive. The procedure was performed using a previously reported synthesis [48,49]. We performed theoretical calculations of the linear (dipole moment and polarizability) and NLO (hyperpolarizabilities β) responses. For β, we are interested in the electric field–induced second harmonic generation, hyper–Rayleigh scattering, and the total hyperpolarizability β_{tot}. We also investigated the frontier molecular orbitals (HOMO and LUMO), their energies, their location, and the nature of these orbitals. The outcomes from this study will be useful for disclosing the structure–properties relationship and provide insights into the nonlinear optical properties of N-octanoyl glycine (**P1**) and N-oleoyl glycine (**P2**). This study will provide guidance on the rational design of new materials with potential properties for NLO and optical devices.

2. Experimental

2.1. Reagents

Oleic chloride (85 %), octanoic chloride (99 %), glycine (99 %), sodium hydroxide (≥99 %, pellets), hydrochloric acid (36.5–38 %), ether (>99.5 %), distilled water was used in the synthetic experiments, was performed out by WATER DISTILLER WRZ-100 rated frequency 50 Hz, rated voltage AC220-240 V, and all other chemicals were obtained from Sigma-Aldrich (Prochima, Tlemcen, Algeria) and were used without further purification. For biological analysis, all chemicals, solvents, and culture media for the antimicrobial evaluation (Nutrient agar, Nutrient broth, Mueller Hinton) used in the present work were obtained from Sigma Aldrich. (Prochima, Tlemcen, Algeria).

Antimicrobial activity of **P1** and **P2** were evaluated against pathogenic strain of bacteria, namely, *Bacillus subtilis subsp*. spizizeniiATCC 6633. It was obtained from the bacteriology laboratory of Pasteur Institute of Oran « Oran, Algeria».

2.2. Instruments and measurements

Structural characterization was performed using readily available analytical methods, including UV–Vis spectroscopy, ^1H, ^{13}C, NMR, FT-IR, and LC-MS. UV–Vis spectroscopy: was carried out by GENESYS 10S UV–Vis spectrophotometer using a 10-mm quartz cell operated at room temperature. ^1H and ^{13}C NMR spectra in $DMSOd_6$ solution were recorded on a BRUKER AC 300P (300 MHz) spectrometer. The IR analyses were carried out on a JASCO4200 Fourier transform IR spectrometer.

Melting point: a Köfler bench was used to determine the melting points for products with a melting temperature below 260 °C.

LC-MS: identification was performed out by electrospray on HPLC waters ALLIANCE2690.

2.3. In vitro antimicrobial activity

The synthesized **P1** and **P2** were examined for their *in vitro* antimicrobial potential against a Gram–positive bacterial strain *Bacillus subtilis* subsp. *Spizizenii*ATCC 6633. The disc diffusion method was modified slightly to assess antimicrobial activity [50].

2.4. Bacterial suspension

The bacterial strain was revivified overnight at 37 °C on Nutrient agar in Petri dishes. The bacterial suspension was prepared for the assays by inoculating 3–4 colonies from the agar plate culture into 10 ml of Nutrient broth and then incubated at 37 °C after 24 h of incubation; the bacterial suspension was standardized to 10^8 CFU/ml using the 0.5 Mc Farland turbidity standards.

2.5. Disc diffusion method

A sterile cotton swab spread the bacterial suspension on Mueller Hinton plates. Whatman No.3 sterile filter paper discs (diameter 6 mm) were impregnated with sterile dilutions of **P1** and **P2** (10, 20, and 30 mg/ml) initially prepared in DMSO following that, the plates were incubated for a day at a temperature of 37 °C. The findings were stated in terms of inhibition zone diameters. All tests were performed in triplicates. Dimethylsulfoxide (solvent) was utilized as a negative control against bacterial strain. Gentamicin was used as a positive control to test the sensibility of the bacteria.

2.6. General procedure for the preparation of N-acyl glycine

The glycine (13.3 mmol, 1 eq) dissolved in an aqueous NaOH solution (13.3 mmol, 1 eq) is added to fatty acids chloride (1.3 mmol, 0.1

eq); the reaction is left under magnetic stirring for 2 h, then the potential of hydrogen of the solution is adjusted to pH = 3 by adding HCl. The resulting products were washed with water and then with ether. The synthetic approach depicted in Scheme 1 below was followed for the construction of **P1** and **P2**.

2.7. Spectroscopic data of *P1*

P1 a crystalline solid. Mp 98 °C (degradation) yield: 93.23 %; ^{1}H NMR (300 MHz, DMSOd$_6$/TMS) δ ppm: 0.85 (t, *J = 7.3 Hz*, 3H, **CH$_3$–**(CH$_2$)$_4$–), 1.12–1.31 (m, 8H, CH$_3$**–(CH$_2$)$_4$–**), 1.47 (t, *J = 7.3 Hz*, 2H, –(CH$_2$)$_4$**–CH$_2$–**CH$_2$), 2.09 (t, *J = 7.4 Hz*, 2H, –CH$_2$**–CH$_2$–**CO), 3.70 (d, *J = 5.9 Hz*, 2H, –NH**–CH$_2$–**CO), 8.11 (t, *J = 5.9 Hz*, 1H, CO**–NH–**CH$_2$–CO) (Fig. S2).

^{13}C NMR (75 MHz, DMSOd$_6$/TMS) δ$_c$ ppm: 14.44, 22.54, 25.66, 28.95, 29.02, 31.66, 35.51, 40.95, 171.96, 173.08 (Fig. S3).

MS (ES$^+$): *m/z* 202.4 [M + H]$^+$, 224.4 [M + Na] +. As seen in Fig. S5 of the LC-MS spectrum of **P1**.

IR (ν_{max}, cm^{-1}, KBr, solid): ν_{OH} = 3303.83 cm^{-1} ν_{CH} = 2918.59 cm^{-1} ν_{COO} = 1694.95 cm^{-1} ν_{CONH} = 1638.87 cm^{-1} (Fig. S4).

UV–visible: UV–Vis spectroscopy of **P1** shows the presence of two bands (Fig. S1).

Band 1: it appears around 280 nm, it corresponds to the transition n → σ*.

Band 2: it appears around 315 nm, it corresponds to the transition n → π*.

2.8. Spectroscopic data of *P2*

P2 is a crystalline solid. Mp 88 °C (degradation) yield: 63.63 %; ^{1}H NMR (300 MHz, DMSOd$_6$/TMS) δ ppm, 0.84 (t, *J = 7.3 Hz*, 3H, **CH$_3$–**(CH$_2$)$_6$), 1.12–1.38 (m, 20H, CH$_3$**–(CH$_2$)$_6$–**CH$_2$–CH = CH–CH$_2$**–(CH$_2$)$_4$–**CH$_2$–), 1.48 (p, *J = 7.1 Hz*, 2H, –CH$_2$**–CH$_2$–**CH$_2$–CO), 1.98 (q, *J = 6.2 Hz*, 4H, **–CH$_2$–**CH = CH**–CH$_2$–**), 2.14 (dt, *J = 23.5, 7.4 Hz*, 2H, –CH$_2$**–CH$_2$–**CO), 3.71 (d, *J = 5.9 Hz*, 2H, –NH**–CH$_2$–**CO), 5.32 (t, *J = 4.9 Hz*, 2H, –CH$_2$**–CH = CH–**CH$_2$), 8.11 (t, *J = 5.9 Hz*, 1H, CO**–NH–**CH$_2$–CO) (Fig. S7).

^{13}C NMR (75 MHz, DMSOd$_6$/TMS) δ$_c$ ppm: 14.41, 22.59, 25.00, 25.66 27.04, 27.09, 29.05, 29.09, 29.19, 29.33, 29.54, 29.59, 29.61, 31.77, 35.50, 40.96, 130.08, 130.13, 171.95, 172.99 (Fig. S8).

MS (ES$^+$): *m/z* 340.4 [M + H]$^+$, 362.4 [M + Na]$^+$. As seen in Fig. S10 of the LC-MS spectrum of **P2**.

IR (ν_{max}, cm^{-1}, KBr, solid): ν_{OH} = 3298.64 cm^{-1} ν_{CH} = 2913.56 cm^{-1} ν_{COO} = 1695.43 cm^{-1} ν_{CONH} = 1640.80 cm^{-1} (Fig. S9).

UV–visible: UV–Vis spectroscopy of **P2** shows the presence of three bands (Fig. S6).

Band 1: it appears around 280 nm, it corresponds to the transition π → π*.

Band 2: it appears around 301 nm, it corresponds to the transition n → σ*.

Band 3: it appears around 312 nm, it corresponds to the transition n → π*.

2.9. Computational details

The optimized geometry of **P1** and **P2** have been performed at the B3LYP/6–311 + G(d,p) using Gaussian 09 [51]. The 6–311 + G(d,p) gives accurate results for these kinds of compounds [30]. Fig. 2 and (Tables S1 and S2) present the optimized geometries and coordinates. The structures and molecular orbitals have been visualized using GaussView 5.1 [52]. The dipole moment μ, isotropic polarizability $\langle\alpha\rangle$, anisotropy of the polarizability $\Delta\alpha$, first order hyperpolarizability β, hyper–Rayleigh scattering (HRS) hyperpolarizability β_{HRS}, electric

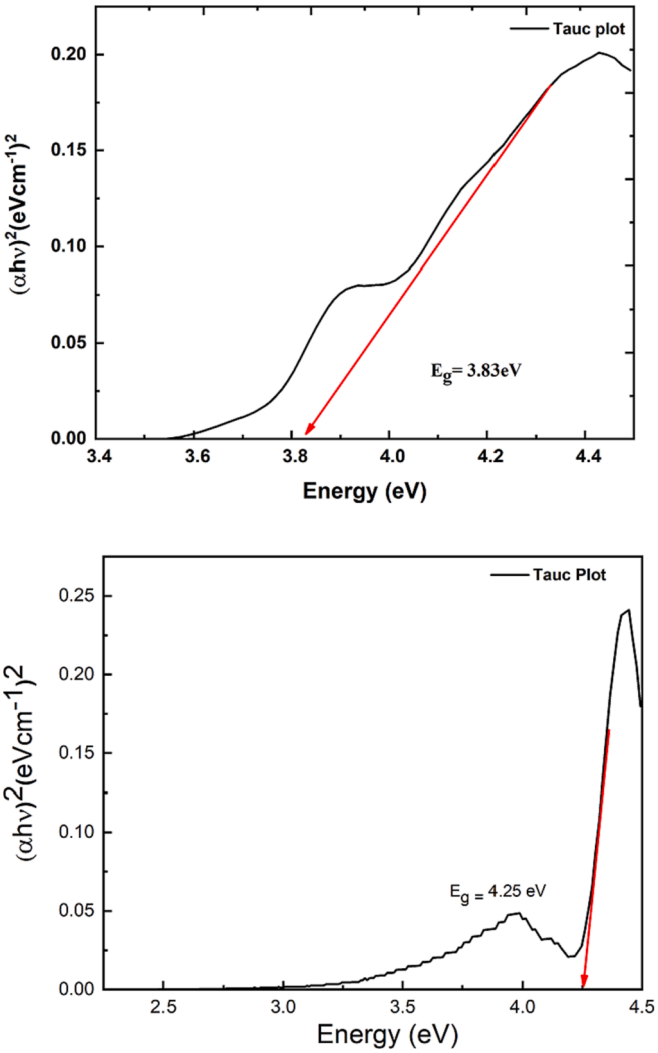

Fig. 1. The absorption spectrum of **P1** (upper panel) and **P2** (lower panel) as a function of the energy.

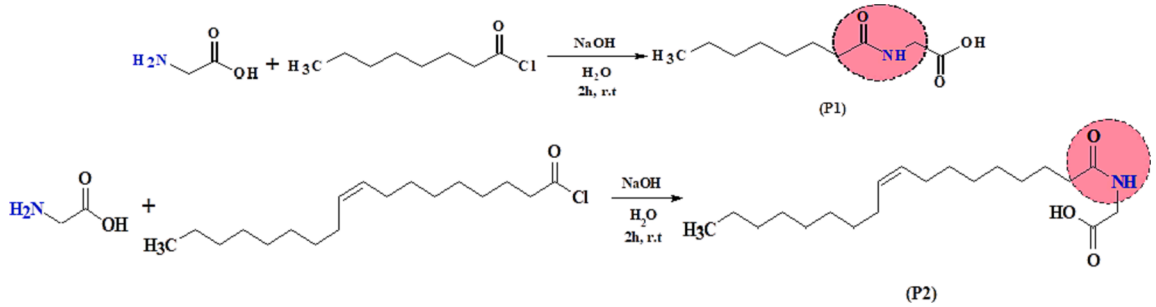

Scheme 1. The synthesis of **P1** and **P2**.

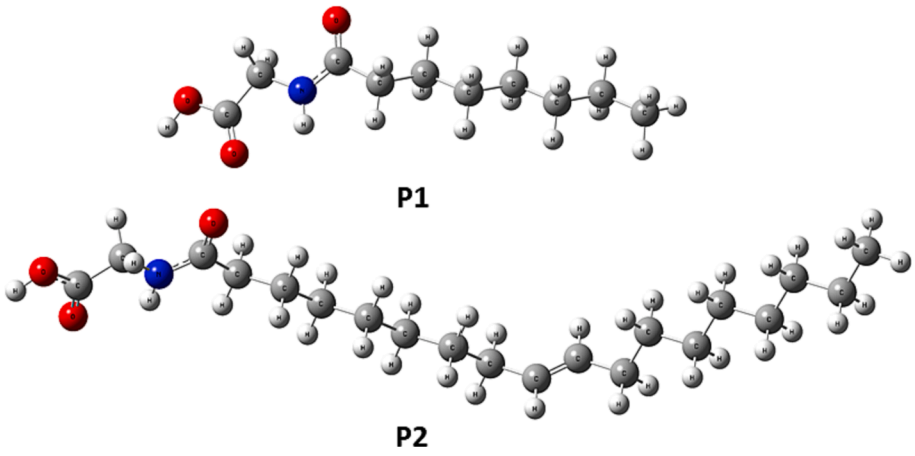

Fig. 2. The optimized structure of **P1** and **P2** obtained using the B3LYP/6–311 + G(d,p) level.

field–induced second harmonic generation (EFISHG) $\beta_{//}$, and the depolarization ratio *DR* are evaluated applying the B3LYP [53,54], PBE0 [55], BVP86 [56,57], ωB97X −D [58] and M06 −2X [59] levels using the 6–311 + G(d,p). Recent work demonstrates the appropriateness of the corrected XC functionals to predict α and β [60]. For medium-sized molecules similar to our N-acyl glycine derivatives, the DFT is usually considered a good choice to calculate α [30]. In the EFISHG, the $\beta_{//}$ is the central quantity, the vector component of β projected along μ axis,

$$\beta_{//}(-2\omega;\omega,\omega)=\beta_{//}=\frac{1}{5}\sum_{i}\frac{\mu_i}{|\vec{\mu}|}\sum_{j}\left(\beta_{ijj}+\beta_{jij}+\beta_{jji}\right) \tag{1}$$

In the static limits, the component $\beta_{ijj}=\beta_{jij}=\beta_{jji}$ and so,

$$\beta_{//}=\frac{3}{5}\sum_{i=x,y,z}\frac{\mu_i\beta_i}{|\vec{\mu}|} \tag{2}$$

$|\vec{\mu}|$: the norm of μ

μ_i and β_i: the i^{th} components of μ and β vectors.

In HRS, *DR* was also calculated. For a non–polarized incident signal, and for the reason that both polarizations are detected with equal sensitivity, the orientational average over β is

$$|\beta_{HRS}|=\sqrt{\langle\beta^2_{HRS}\rangle}=\sqrt{\langle\beta^2_{ZZZ}\rangle+\langle\beta^2_{ZXX}\rangle} \tag{3}$$

and

$$DR=\frac{I^{2\omega}_{VV}}{I^{2\omega}_{HV}}=\frac{\langle\beta^2_{ZZZ}\rangle}{\langle\beta^2_{ZXX}\rangle} \tag{4}$$

The $\langle\beta^2_{ZZZ}\rangle$ and $\langle\beta^2_{ZXX}\rangle$ are orientational averages of β components, describing the HRS intensities when the incident light is vertically or horizontally polarized, respectively. The $\langle\beta^2_{ZZZ}\rangle$ and $\langle\beta^2_{ZXX}\rangle$ are calculated as [61]:

$$\begin{aligned}\langle\beta^2_{ZZZ}\rangle=&\frac{1}{7}\sum_{\zeta}^{x,y,z}\beta^2_{\zeta\zeta\zeta}+\frac{4}{35}\sum_{\zeta\neq\eta}^{x,y,z}\beta^2_{\zeta\zeta\eta}+\frac{2}{35}\sum_{\zeta\neq\eta}^{x,y,z}\beta_{\zeta\zeta\zeta}\beta_{\zeta\eta\eta}+\frac{4}{35}\sum_{\zeta\neq\eta}^{x,y,z}\beta_{\eta\zeta\zeta}\beta_{\zeta\zeta\eta}\\&+\frac{4}{35}\sum_{\zeta\neq\eta}^{x,y,z}\beta_{\zeta\zeta\zeta}\beta_{\eta\eta\zeta}+\frac{1}{35}\sum_{\zeta\neq\eta}^{x,y,z}\beta^2_{\eta\zeta\zeta}+\frac{4}{105}\sum_{\zeta\neq\eta\neq\varepsilon}^{x,y,z}\beta_{\zeta\zeta\eta}\beta_{\eta\varepsilon\varepsilon}+\frac{1}{105}\sum_{\zeta\neq\eta\neq\varepsilon}^{x,y,z}\beta_{\eta\zeta\zeta}\beta_{\eta\varepsilon\varepsilon}\\&+\frac{4}{105}\sum_{\zeta\neq\eta\neq\varepsilon}^{x,y,z}\beta_{\zeta\zeta\eta}\beta_{\varepsilon\varepsilon\eta}+\frac{2}{105}\sum_{\zeta\neq\eta\neq\varepsilon}^{x,y,z}\beta^2_{\zeta\eta\varepsilon}\\&+\frac{4}{105}\sum_{\zeta\neq\eta\neq\varepsilon}^{x,y,z}\beta_{\zeta\eta\varepsilon}\beta_{\eta\zeta\varepsilon}\end{aligned} \tag{5}$$

$$\begin{aligned}\langle\beta^2_{XZZ}\rangle=&\frac{1}{35}\sum_{\zeta}^{x,y,z}\beta^2_{\zeta\zeta\zeta}+\frac{4}{105}\sum_{\zeta\neq\eta}^{x,y,z}\beta_{\zeta\zeta\zeta}\beta_{\zeta\eta\eta}-\frac{2}{35}\sum_{\zeta\neq\eta}^{x,y,z}\beta_{\zeta\zeta\zeta}\beta_{\eta\eta\zeta}+\frac{8}{105}\sum_{\zeta\neq\eta}^{x,y,z}\beta^2_{\zeta\zeta\eta}\\&+\frac{3}{35}\sum_{\zeta\neq\eta}^{x,y,z}\beta^2_{\zeta\eta\eta}-\frac{2}{35}\sum_{\zeta\neq\eta}^{x,y,z}\beta_{\zeta\zeta\eta}\beta_{\eta\zeta\zeta}+\frac{1}{35}\sum_{\zeta\neq\eta}^{x,y,z}\beta_{\zeta\eta\eta}\beta_{\zeta\varepsilon\varepsilon}\\&-\frac{2}{105}\sum_{\zeta\neq\eta\neq\varepsilon}^{x,y,z}\beta_{\zeta\zeta\eta}\beta_{\eta\varepsilon\varepsilon}+\frac{2}{35}\sum_{\zeta\neq\eta\neq\varepsilon}^{x,y,z}\beta^2_{\zeta\eta\varepsilon}-\frac{2}{105}\sum_{\zeta\neq\eta\neq\varepsilon}^{x,y,z}\beta_{\zeta\eta\varepsilon}\beta_{\eta\zeta\varepsilon}\end{aligned} \tag{6}$$

3. Results and discussion

3.1. Antimicrobial activity

The results obtained on antimicrobial evaluation of the synthesized compounds are presented in Table 1.

The antimicrobial activities of the N-acyl amino acids prepared in this study were evaluated against pathogenic organisms, Gram positive and catalase positive bacterium. *Bacillus subtilis* subsp. *spizizenii*ATCC 6633 was utilized to study the ability of **P1** and **P2** at 10, 20, and 30 mg/ml concentration to inhibit microbial growth. The bacterial species were incubated overnight at 37 °C on nutrient broth. **P1** and **P2** exhibited a good level of activity against the tested organisms. Table 1 shows the activity of **P1** and **P2** against the *Bacillus subtilis* subsp. *Spizizenii*ATCC 6633.

Observing the overall data for antimicrobial activity, for **P1**, there is a progressive decrease in inhibition zones with increasing concentration, going from 10.25 ± mm at 10 mg/ml to 8.25 ± mm at 20 mg/ml, and further to 7 ± mm at 30 mg/ml suggests potential concentration dependence, where higher concentrations might reduce the inhibitory effect. The bacterial growth is unaffected or even stimulated by the increase in concentration, and This could be due to several factors: the inactivation property of this type of bacteria by an enzyme that degrades the synthesized compound and reduces its effectiveness, the saturation

Table 1
Antimicrobial evaluation of **P1** and **P2** after 24 h, with means of inhibition zones ± sd.

Bacterial strain	*Bacillus subtilis subsp.* spizizeniiATCC 6633		
Compounds	Inhibition zones diameter (mm)		
	10 mg/ml	20 mg/ml	30 mg/ml
P1	10.25±	8.25±	7±
P2	7.33±	8.16±	11.5±
Negative control (DMSO)	6.5±	6.5±	6.5±
Positive control (Gentamycine)	25±	33.5±	25±

NB: Inhibition zones are including the disc diameter (6 mm).

of the active sites on the bacterial cells, and the adaptation of the bacteria by developing resistance mechanisms to increase their ability to eliminate the chemical compound. Also, *B. subtilis* can split symmetrically to make two daughter cells or asymmetrically, forming a tough, single protective endospore at times of nutritional stress and allowing the organism to persist in the environment until conditions become appropriate. Bacterial growth can also be affected by environmental parameters such as pH, salinity, and temperature [62,63]. These effects remain the characteristics and the action mechanisms of **P1** and **P2**, which determine their effectiveness against bacteria and provide the best strategy to prevent bacterial resistance. In contrast, for **P2**, the results showed an interesting variation. At 10 mg/ml, the inhibition zone is 7.33 ± mm, increasing to 8.16 ± mm at 20 mg/ml and reaching a maximum of 11.5 ± mm at 30 mg/ml. This significant increase at the highest concentration implied potential positive concentration dependence, indicating that the inhibitory effect of **P2** might be favored at higher concentrations. Comparing the two compounds, at the highest concentration (30 mg/ml), **P2** exhibited a larger inhibition zone than **P1** (11.5 ± mm compared to 7 ± mm), suggesting that **P2** could have a stronger inhibitory effect at this specific concentration.

The apparent differences in **P1** and **P2** inhibitions depended on the length of the fatty chain, the mode of attachment of the amino acid, and the position of the acid function. The inhibitory impact seen may be attributed to the presence of amide linkages, wherein a stronger hydrogen connection links the –NH group of the amino acids and the oxygen of the fatty moiety, which could potentially lead to an increased rate of antimicrobial activity. The phenomenon referred to as the hydrogen belt effect plays a role in the hindrance of antibacterial activity [15]. As expected, antimicrobial action was strongly correlated with the long-chain N-acyl amino acid, which is more potent than short-chain N-acyl amino acids [24]. Loss of effectiveness could occur if the fatty acid chain is too short and the lipoaminoacid interacts unfavorably with components of the bacterial cell membrane. These findings are in accordance with our study's results and previous studies [64,65]. According to Storck *et al.* [66], the modification of synthetic antibacterial peptides Pep19-4LF with lengthy fatty acids can be a tool for improving the characteristics of antimicrobial peptides. Furthermore, Sreenu *et al.* [67] illustrate that the sodium N-palmitoyl amino acids synthesized using the Schotten-Baumann reaction with 16 chain-length carbon atoms exhibited good antimicrobial efficacy against *S. aureus MLS-16* and *Bacillus subtilis*. Other researchers [15] have reported that the N-Stearoyl amino acids with 18 chain-length carbon atoms may be more potent against different bacterial strains such as *Staphylococcus aureus*, *Micrococcus luteus*, and *Bacillus cerceus*, *Escherichia coli* and *Pseudomonas aeruginosa*, and the yeast *Candida albicans*. Another approach [68] has dealt with long-chain N-acyl amino acid antibiotics isolated directly from soil samples and found that C13 to C16 saturated and unsaturated N-acyl substituted L-tyrosines were the most active against *B. subtilis*. In line with these findings, and in our study, for high concentrations (30 mg/ml), **P2** with a lengthy fatty chain (C18) and one unsaturation in the carbon backbone showed higher (11.5 ±) antimicrobial activity compared to **P1** with short-chain fatty (C8) (7 ±).

3.2. Linear and NLO results

3.2.1. Dipole moment

The μ of a molecule refers to its electrical response feature, which arises due to the uneven distribution of charges among the atoms of the molecule [69]. Table 2 presents the variations in μ values for our N-acyl glycine derivatives, determined by the utilization of five different DFT functionals at the 6–311 + G(d,p) basis set. μ and $\langle\alpha\rangle$ were evaluated utilizing ωB97X −D, B3LYP, PBE0, M06 −2X and BVP86 levels. The calculated μ values of **P1** vary between 2.47 and 2.49 D, whereas μ of **P2** varies between 2.43 and 2.46 D. Inspection of Table 2 shows that the μ values are convergent, as the value of μ increases, there is an associated increase in α value. Additionally, when μ is high, the same relationship holds true, and therefore $\langle\alpha\rangle$ is high. **P1** possesses a high μ. In turn, **P2** has the highest $\langle\alpha\rangle$. An accurate analysis of these results shows that the PBE0 and BVP86 functionals give the highest μ value. Whereas, the B3LYP, ωB97X −D, and M06 −2X exchange–correlation (XC) functionals show systematically smaller μ values. PBE0, BVP86, and M06 −2X show similar μ (less than 1 %) for **P1**, while we have gotten the subsequent variations. For **P2**, and compared to PBE0 functional as a reference: 0.4 % for BVP86, 1.21 % for (B3LYP, M06 −2X and ωB97X −D). The obtained μ results indicated that our derivatives **P1** and **P2** have reasonably good NLO behavior. The μ values are very convergent. N-acyl glycine derivative **P1**, with short-chain fatty (C8), has a larger μ of 2.49 D compared to **P2** (2.46 D), which has a lengthy fatty chain (C18). The calculated μ values show high polarity for **P1** compared with **P2**, indicating a reasonable NLO behavior. In the case of **P2**, where the bridge length increases, there is a relative decrease in the observed μ values (Table 2). The ordering of μ values is as follows:

$$\mu_{B3LYP} \leq \mu_{\omega B97X-D} < \mu_{PBE0} \leq \mu_{BVP86} \leq \mu_{M06-2X}$$

$$\mu_{P2} < \mu_{P1}$$

To make an accurate assessment, we have compared our results with experimental values for a similar compound, N-acetyl-DL-methionine, and with the urea [70] and *p*–nitroaniline [71] reference molecules. A direct correlation has been obtained between the biological activity and the dipole moment. Our analysis demonstrates that the most important factors that affect the antimicrobial activity are the descriptors like

Table 2
μ, $\langle\alpha\rangle$, $\Delta\alpha$, β_{tot}, $\beta_{//}$, β_{HRS}, and *DR* for **P1** and **P2** obtained using five DFT approaches at the 6–311 + G(d,p) basis set. Comparisons with experimental and the B3LYP/6–311 + G(d,p) results.

		μ	$\langle\alpha\rangle$	$\Delta\alpha$	$\beta_{//}$	β_{tot}	β_{HRS} ***(DR)***
B3LYP	**P1**	2.47	136.21	59.65	23.30	78.54	35.11 (3.72)
	P2	2.43	259.66	122.92	43.89	111.12	44.86 (5.47)
		2.01[a]	62.08 [a]	10.62 [a]		250.66 [a]	
PBE0	**P1**	2.49	142.70	67.54	72.77	154.23	58.48 (4.68)
	P2	2.46	271.10	136.64	109.51	207.62	82.06 (5.94)
BVP86	**P1**	2.49	142.11	66.69	66.98	144.90	63.21 (3.09)
	P2	2.45	270.33	135.45	106.63	203.05	80.82 (5.83)
ωB97X–D	**P1**	2.47	133.25	54.88	–3.17	71.76	34.20 (3.48)
	P2	2.43	254.32	114.55	15.62	110.49	45.88 (4.94)
M06–2X	**P1**	2.49	132.01	54.39	–3.06	69.60	34.14 (3.30)
	P2	2.43	252.60	114.86	13.32	101.09	44.15 (4.35)
		4.56[b]				43[b]	
		6.2 [c]					

[a] [30] Results for similar compound obtained at the B3LYP functional.
[b] [70] Experimental values for urea.
[c] [71] Experimental values for *p*-nitroaniline.

HOMO, LUMO, and μ [72]. The results indicated that **P1** with the highest μ values exhibits a strong inhibitory action, whereas the effectiveness of **P2** with the lowest μ values against bacterial growth. A similar assessment has been showed in a recent study [73]. The biological activity of lipoaminoacids increases with the decrease of μ, E_g, as well as the increase of their polarizabilities. Our results support the previous findings [72,73], which show that compounds with lower μ are more potent than compounds with a higher μ, indicating that the dipole moment is not solely responsible for modulating the biological activity. Other parameters, such as hydrophobicity, hydrophilicity, cell permeability, and cell membrane interaction, can also affect the activity [73].

3.2.2. Polarizability

$\langle\alpha\rangle$ was calculated using x_{ij} components by the formula

$$\langle\alpha\rangle = \frac{1}{3}\left(\alpha_{xx} + \alpha_{yy} + \alpha_{zz}\right) \tag{7}$$

and $\Delta\alpha$ by the formula:

$$\Delta\alpha = \sqrt{\frac{1}{2}\left[\left(\left(\alpha_{xx} - \alpha_{yy}\right)^2 + \left(\alpha_{xx} - \alpha_{zz}\right)^2 + \left(\alpha_{yy} - \alpha_{zz}\right)^2\right)\right]} \tag{8}$$

The computation was performed using multiple DFT approaches at the 6–311 + G(d,p) basis set. Table 2 exhibits α and β values of **P1** and **P2**. Examining Table 2 reveals that ⟨α⟩ increases gradually when passing from the B3LYP, M06 −2X, and ωB97X −D functionals to PBE0 and BVP86 levels. There is relatively little difference in ⟨α⟩ and $\Delta\alpha$ between the corrected functionals BVP86 and PBE0 with comparison to the reported variations among the other DFT approaches under investigation. The high $\langle\alpha\rangle$ value of **P1** is achieved with the PBE0. Its value equals to 142.70 a.u. The same trend is observed for **P2**, where the calculated $\langle\alpha\rangle$ value equals to 271.10 a.u. at the same PBE0 level. This is commensurate with the work of Adamo *et al.* [55], who assert that the PBE0 is probably the best functional currently available for α calculations. Furthermore, exposed research [73] demonstrated that the PBE0 exaggerates $\langle\alpha\rangle$ for forty–six chemicals. The same assessment has been obtained by Paidarová *et al.* [74]. A similar observation was seen in the study conducted by Sabirov [75], which showed the accuracy of the PBE0 model to reproduce the α values of C_{60}. So, the same finding was obtained in this study. α values for both **P1** and **P2** follow the ordering:

$$\langle\alpha\rangle_{\text{M06–2X}} < \langle\alpha\rangle_{\text{ωB97X–D}} < \langle\alpha\rangle_{\text{B3LYP}} < \langle\alpha\rangle_{\text{BVP86}} < \langle\alpha\rangle_{\text{PBE0}}$$
$$\Delta\alpha_{\text{M06–2X}} < \Delta\alpha_{\text{ωB97X–D}} < \Delta\alpha_{\text{B3LYP}} < \Delta\alpha_{\text{BVP86}} < \Delta\alpha_{\text{PBE0}}$$

When comparing $\langle\alpha\rangle$ values obtained with the PBE0 functional as a reference with that obtained with different computational levels for **P1**, the deviations obtained are 0.49 % for BVP86, ~5% for B3LYP, 6.62 % for ωB97X −D and 7.49 % M06 −2X. For $\Delta\alpha$, we obtain the following deviations: 0.29 % for BVP86, ~4% for B3LYP, ~6% for ωB97X −D, and ~ 7 % M06 −2X functional. The polarizability values of **P2** are computed to be greater than that of **P1**, the α does not show a significant effect of the length of the fatty chain. The highest calculated $\langle\alpha\rangle$ and $\Delta\alpha$ polarizabilities were found to be 271.10 and 136.64 a.u for **P2**, i.e., ~5 and ~ 13 times higher than the urea [70], respectively. Whereas the computed high values of $\langle\alpha\rangle$ and $\Delta\alpha$ were found to be 142.70 and 67.54 a.u for compound, which are ~ 3 and ~ 7 times higher than urea [70]. The same assessment was obtained in varying proportions with the standard *para*-nitroaniline (*p*NA) [71].

$$\langle\alpha\rangle\ \mathbf{P2} > \langle\alpha\rangle\ \mathbf{P1}$$
$$\Delta\alpha\ \mathbf{P2} > \Delta\alpha\ \mathbf{P1}$$

3.2.3. Hyperpolarizability

The β parameter provides indications regarding the optical nonlinearity exhibited by the molecular system and is typically associated with the intramolecular charge transfer. $\beta_{//}$ and β_{HRS} of **P1** and **P2** have been

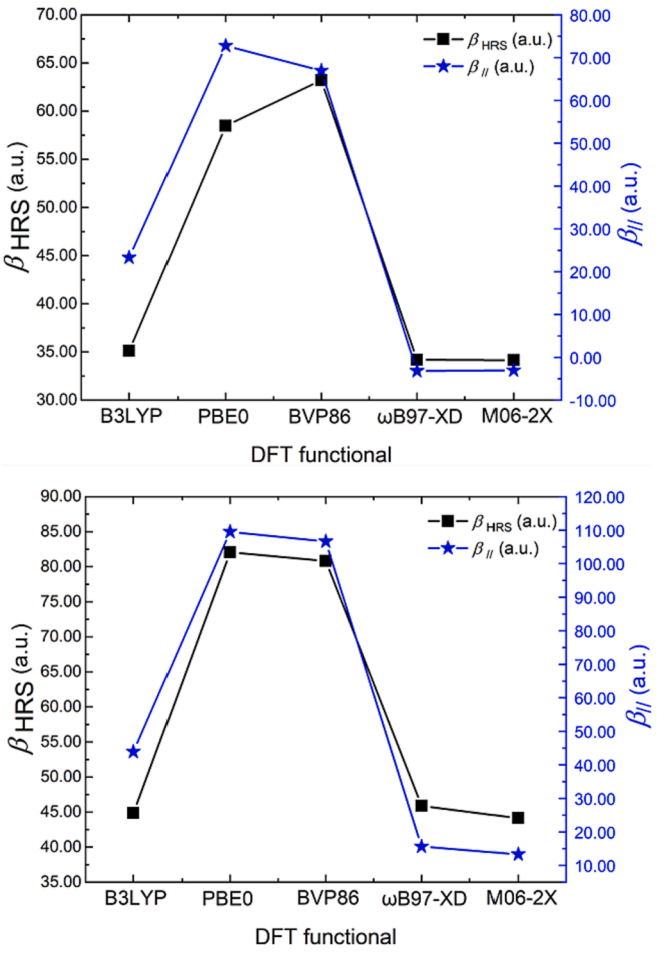

Fig. 3. β_{HRS} and $\beta_{//}$ of **P1** (upper panel) and **P2** (lower panel) calculated using five functionals with 6–311 + G(d,p) basis set.

computed at different DFT approaches (PBE0, B3LYP, ωB97X −D, BVP86, and M06 −2X). The obtained results are regrouped in Fig. 3 and Table 2. Based on the predicted β values, high β_{HRS} values have been obtained for at DFT functionals, including a minimal amount of HF exchange. In contrast, the XC DFT levels that incorporate higher proportions of HF exchange, like B3LYP, M06 −2X, and ωB97X −D give the lowest β_{HRS} values. In comparison to the B3LYP hybrid functional, which has the least amount of 20 % HF exchange, the PBE0 and BVP86 values are smaller, while readings exhibit strong similarity. The highest β_{HRS} value (63.21 a.u.) for **P1** is obtained using the BVP86, whereas the PBE0 method with 40 % of HF exchange provides the highest β_{HRS} (82.06 a.u.) for **P2**. The M06 −2X Minnesota level with 54 % HF exchange provides the smallest β_{HRS} (34.14 and 44.15 a.u.) for **P1** and **P2**, respectively. The calculated β values for both N-acyl glycine derivatives (Table 2) are larger than β values of urea. The high β values of **P2** compared to **P1** are attributable to the strong migration of electrons between the two sides of the N-acyl glycine derivative (amide-the chain-methyl donor), which was significantly increased by the existence of the double bond in the chain of **P2**. Moreover, the carbonyl oxygen of the amides acts as a hydrogen bond acceptor, and the NH of the amides behave as a hydrogen bond donor. In fact, the length of the chain, the position, and the number of carbon–carbon double bond do not just affect the intramolecular charge transfer and the NLO properties, they affect the whole proprieties of the derivatives [29,76,77]. This increase in β_{HRS} could be attributed to an increased μ as well as a decreased band gap (E_g). The (PBE0 and BVP86) and M06 −2X levels offer the smallest and the largest $\beta_{//}$ values, respectively. The β_{HRS} and $\beta_{//}$ have been found to be directly correlated. The same assessment has been obtained in several studies

[78–82]. For more clarity, we could suggest an increasing/decreasing classification relative to the β_{HRS} and $\beta_{//}$, severally. Below is the established order:

For **P1**: $\beta_{HRS\ M06-2X} < \beta_{HRS\ \omega B97X-D} < \beta_{HRS\ B3LYP} < \beta_{HRS\ PBE0} < \beta_{HRS\ BVP86}$
$\beta_{//\ \omega B97X-D} > \beta_{//\ M06-2X} > \beta_{//\ B3LYP} > \beta_{//\ BVP86} > \beta_{//\ PBE0}$
For **P2**: $\beta_{HRS\ M06-2X} < \beta_{HRS\ B3LYP} < \beta_{HRS\ \omega B97X-D} < \beta_{HRS\ BVP86} < \beta_{HRS\ PBE0}$
$\beta_{//\ \omega B97X-D} > \beta_{//\ M06-2X} > \beta_{//\ B3LYP} > \beta_{//\ BVP86} > \beta_{//\ PBE0}$
$\beta_{tot\ P1} < \beta_{tot\ P2}$
$\beta_{HRS\ P1} < \beta_{HRS\ P2}$

The β_{tot} values ranged between 69.60 and 154.23 a.u. for **P1** and, at the same time, ranged between 101.09 and 207.62 a.u. for **P2**. Opposite variations were obtained between β_{tot} and E_g. High β_{HRS} has been achieved at the lower E_g. Similar ascertainment has been obtained in combined experimental and theoretical studies [83,84]. The best maximization for β_{tot} is given for **P2** using the PBE0/6–311 + G(d,p) obtained at lower E_g. The studies showed that molecular symmetry and conjugation are a key part of the electrical properties of molecules and determining the conductance of the molecule. The push–pull effect was visible in both **P1** and **P2**, which was confirmed by lowest E_g and high β values. The obtained results exhibit a satisfactory level of agreement with the experimental values as determined using UV–Vis measurements (Fig. 1 and Table 3) and for similar compound [30]. The depolarization ratio *DR* provides the molecular geometry information, which depends on the symmetry of the molecular scatterer and ranges from 3.09 to 4.68 for **P1**, and from 4.35 to 5.94 for **P2** (Table 2). These *DR* values are congruent with the topology of one–dimensional N-acyl glycine systems.

3.3. Frontier molecular orbital (FMO) analysis

In this part of our assessment, we have studied the two frontier molecular orbitals (Fig. 5) and their E_g (Fig. 4, and Table 3) which are crucial in a diverse array of chemical reactions commonly shortened HOMO and LUMO [85,86]. The E_g of the two N-acyl glycine derivatives is obtained by analysing the UV–Vis spectrum presented in Fig. S1 and Fig. S6. Maximum absorption of around 4 eV near–UV region was noticed, which highlights the $\pi \rightarrow \pi^*$ transition between the HOMO and LUMO of these acyl glycine derivatives. As shown in Fig. S1 and Fig. S6, the UV–Vis analysis provides confirmation that the acyl glycine derivatives have favorable optical absorption characteristics, including adjustable intensity and absorption areas. Fig. 1 displays evolution curves of the absorption coefficient as a function of incident energy. In light of these figures, we used a Tauc plot method to compute E_g [87] depending on the adjustment of *x*-axis intercept, which equals about

Table 3
E_{HOMO}, E_{LUMO}, E_g in eV and β_{tot} in a.u. of **P1** and **P2** obtained using five DFT approaches at the 6–311 + G(d,p) basis set. Comparisons with experimental (in parentheses) and with the B3LYP results for a similar compound.

		E_{HOMO}	E_{LUMO}	E_g	β_{tot}
B3LYP	**P1**	–7.08	–0.66	6.42	78.54
	P2	–6.59	–0.66	5.93 5.32 [a]	111.12
PBE0	**P1**	–5.69	–1.53	4.16 (3.98)	154.23
	P2	–5.66	–1.53	4.13 (4.25)	207.62
BVP86	**P1**	–5.79	–1.61	4.18	144.90
	P2	–5.75	–1.61	4.14	203.05
ωB97X–D	**P1**	–9.28	1.49	10.07	71.76
	P2	–8.64	1.49	10.13	110.49
M06–2X	**P1**	–9.03	0.80	9.83	69.60
	P2	–8.11	–0.80	7.31	101.09

[a] [30] E_g for the N-acetyl-DL-methionine at the B3LYP approach.

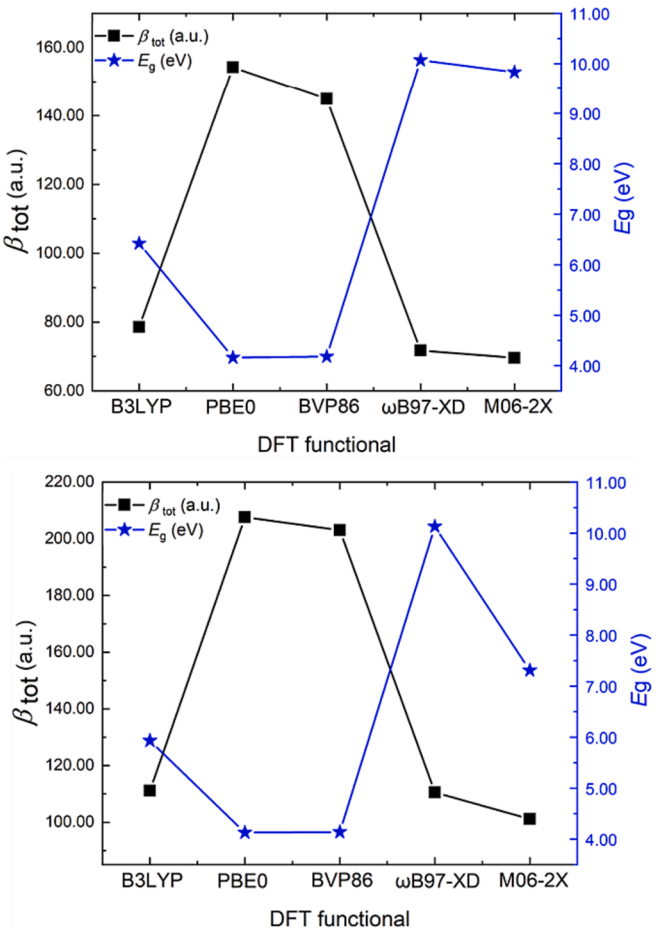

Fig. 4. β_{HRS} and E_g of **P1** and **P2** determined at five DFT levels using the 6–311 + G(d,p) basis set.

3.98 and 4.25 eV for **P1** and **P2**, respectively. The HOMO and LUMO energy of these glycines are negative, and these glycines are stable.

The E_g of the studied N-acyl glycine derivatives varied from 4.16 to 10.07 eV and from 4.13 to 10.13 eV using the PBE0 and ωB97X–D functionals for both **P1** and **P2**, respectively (Table 3 and Fig. 4), which implies that the N-acyl glycine derivatives are able to take a low value of E_g to transfer electrons from HOMO to LUMO. The low E_g is attributed to N–oleoyl glycine with a minor difference in N–octanoyl glycine values.

The lowest E_g values are 4.16 and 4.13 eV for both **P1** and **P2** were acquired by the PBE0/6–311 + G(d,p) level. This functional gives E_g value close to that of the experimental. Using the same B3LYP level, our E_g results were close to those obtained for the N-acetyl-DL-methionine [30], a difference of 17 % was recorded. The frontier molecular orbitals analysis of **P1** and **P2** showed that the LUMO is located over the carboxyl group, this is shown by all B3LYP, PBE0, BVP86, ωB97X–D, and M06–2X levels. The same assessment was shown by Günay *et al.* [30] in their study of the structure, orbitals, and NLO properties of the N-acetyl-DL-methionine. The authors showed that the HOMO in the N-acetyl-DL-methionine is localized over the -$C_5H_2SC_6H_3C_7H_2$ chain, while the LUMO is located over the carboxyl group. Also, like our compounds, and according to Li *et al.* [88], the LUMO is located over the carboxyl group in the glycine oligopeptides. In our **P1** and **P2**, the HOMO is localized on the carboxamide HN-C = O in the case of **P1** and on the HC = CH bound in the case of **P2** with a weak participation of p_z orbitals of C atoms of the rest of the chain. FMO is a valuable tool for qualitative descriptions of biological activity and an important stability index that helps characterize the molecules chemical reactivity, kinetic stability, and optical polarizability [89]. The key characteristics of a molecule in FMO theory

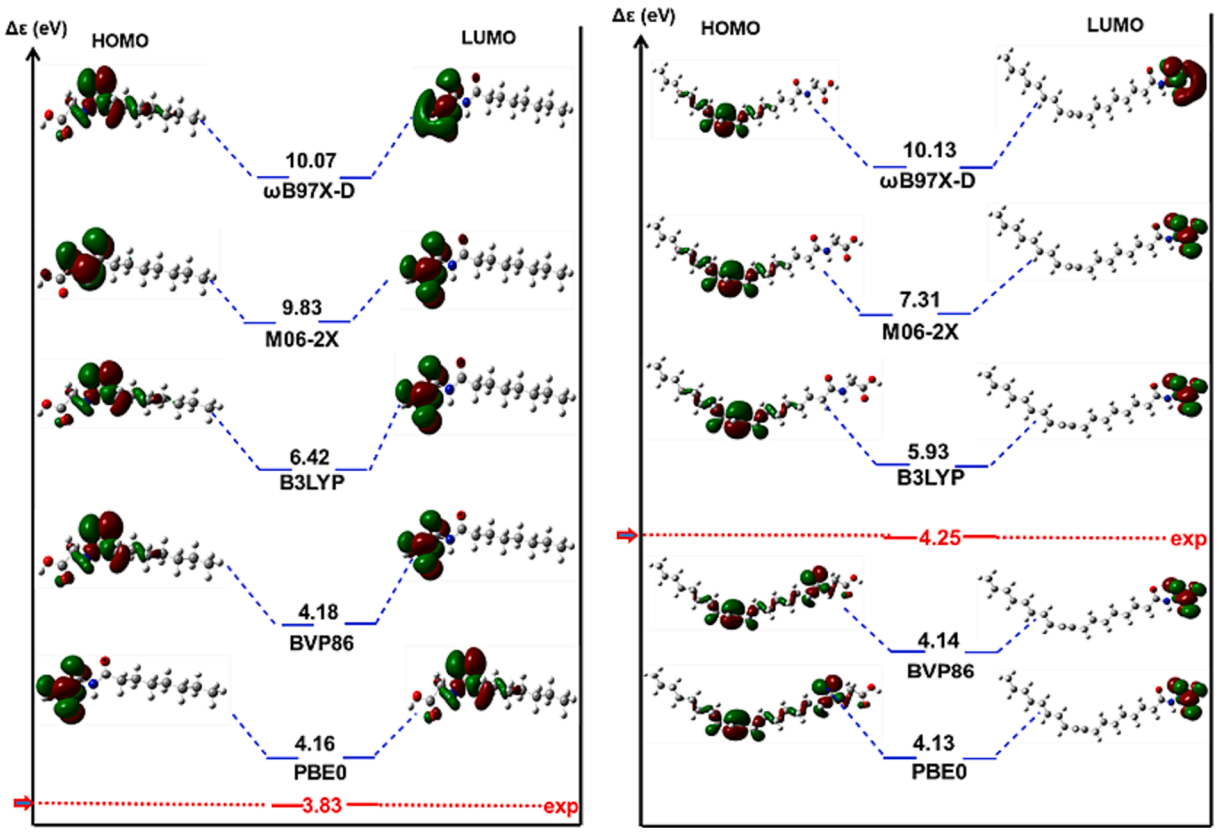

Fig. 5. HOMO, LUMO, and E_g in eV of **P2** (right) and **P1** (left) determined at five DFT levels using the 6–311 + G(d,p) basis set.

are the difference between the energies of E_{HOMO} and E_{LUMO} (E_g), global hardness, and softness of the system, which are treated as descriptors. A molecule with a small E_g is more polarized and characterized by greater bioactivity, high chemical reactivity, and low kinetic stability, known as a soft molecule [90,91]. Soft molecules are more reactive than hard ones because they easily offer electrons to an acceptor. The small E_g indicates that charge transfer easily occurs in it, which influences the biological activity of the molecules [92]. The E_{HOMO} and E_{LUMO} and the descriptive properties of **P1** and **P2**, such as the chemical hardness (η) [93], chemical potential (V), chemical softness (S), electronegativity (χ), electrophilicity index (ω), electron affinity (A), and nucleophilicity index (N) [94,95] are calculated at the same DFT levels and regrouped in Table 4. These descriptors were evaluated from the following equations:

$$A = -E_{LUMO}; I = -E_{HOMO}; V = (I+A)/2; S = 1/2\eta$$

$$\eta = (-A+I)/2; \chi = (I+A)/2; \omega = V^2/2\eta; N = 1/\omega$$

The η and E_g values demonstrate the intramolecular charge transfer inhibition [96]. The stability is confirmed by the large η values of **P1** and **P2**, which are 5.38 and 5.06 eV, respectively. The computed large η and small E_g values for **P2** exhibits promising charge transfer in the molecule, proving that these N-acyl glycine derivatives are biologically active.

The ω index [97] is related to the stabilization of energy when the system gains an additional electronic charge from the surroundings and quantifies the global electrophilic power of the molecule [98]. The FMO study indicates that **P2** has the lowest E_g (4.13 eV), meanwhile, the **P1** possesses the highest E_g (4.16 eV). The lower E_g in **P2** demonstrates the inevitable charge transfer. **P2** has more reactive HOMO (E_{HOMO} = − 5.66 eV), and **P1** has less reactive HOMO (E_{HOMO} = − 5.69 eV). The LUMO with the least energy is present in **P2** (E_{LUMO} = − 1.61 eV) and with high energy in **P1** (E_{LUMO} = –1.49 eV). The N-acyl glycine with the highest V is **P1** (V = 9.28 eV), and the lowest V value was obtained for **P2** (V = 5.75 eV). The electron affinity A value is higher for **P2** (A = 1.61 eV) and is lower for **P1** (A = –1.49 eV). During molecular interactions, the LUMO accepts electrons, and its E_{LUMO} corresponds to the electron

Table 4
The E_{HOMO}, E_{LUMO}, E_g, I, A, η , χ, ω in eV, S, V in eV^{-1}, and N of **P1** and **P2** computed at five levels using the 6–311 + G(d,p) basis set.

		E_{HOMO}	E_{LUMO}	E_g	I	A	χ	η	S	V	ω	N
B3LYP	**P1**	–7.08	–0.66	6.42	7.08	0.66	3.87	3.21	0.15	3.87	2.33	0.42
	P2	–6.59	–0.66	5.93	6.59	0.66	3.62	2.96	0.16	3.62	2.21	0.45
PBE0	**P1**	–5.69	–1.53	4.16	5.69	1.53	3.61	2.08	0.240	3.61	3.13	0.31
	P2	–5.66	–1.53	4.13	5.66	1.53	3.59	2.06	0.242	3.59	3.12	0.32
BVP86	**P1**	–5.79	–1.61	4.18	5.79	1.61	3.7	2.09	0.23	3.7	3.27	0.30
	P2	–5.75	–1.61	4.14	5.75	1.61	3.68	2.07	0.24	3.68	3.27	0.30
ωB97X–D	**P1**	–9.28	1.49	10.07	9.28	–1.49	3.89	5.38	0.092	3.89	1.40	0.71
	P2	–8.64	1.49	10.13	8.64	–1.49	3.57	5.06	0.098	3.57	1.25	0.80
M06–2X	**P1**	–9.03	0.80	9.83	9.03	–0.80	4.11	4.91	0.10	4.11	1.72	0.58
	P2	–8.11	–0.80	7.31	8.11	0.80	4.45	3.65	0.13	4.45	2.71	0.36

affinity, while the HOMO represents electron donors and its E_{HOMO} is associated with the ionization potential [99]. The evaluated E_g are found to be 4.16 and 4.13 eV for **P1** and **P2**, respectively obtained using the PBE0/6–311 + G(d,p) level (Table 3). The E_g indicates that **P2** is a softest compared to **P1**, while the E_{HOMO} and E_{LUMO} values are mostly negative, which confirms the stability of the prepared N-acyl glycine derivatives [100]. A wider E_g refers to higher stability in the molecular structure. Higher stability points lower chemical reactivity, which means easier replacement of electron distribution. A wider E_g (case of **P1**) indicates greater stability in the molecular structure, whereas a narrower E_g (case of **P2**) refers to chemical softness [101]. The biological reactivity of soft molecules (**P2**) is higher than hard molecules. Conversely, a good electrophile is described by a higher ω value, and the lower ω value denotes a good nucleophile. Our findings suggest that the N-acyl glycine derivatives **P1** and **P2** had larger ω values, indicating a greater propensity to accept electrons and would undergo nucleophilic attack easily. According to the absolute scale of electrophilicity based on the ω index, these chemicals may be classified as strong electrophiles with $\omega > 1.5$ eV, moderate electrophiles with $0.8 < \omega < 1.5$ eV, and marginal electrophiles with $\omega < 0.8$ eV [102]. The same behavior was noticed in compounds recently reported [32]. The strong electrophilic nature of our N-acyl glycine derivatives supports their usability as bioactive substances [103]. The outcomes from this study will be useful for disclosing the structure–properties relationship and provide insights into the electronic structure of N-acyl glycine derivatives, including the distribution of electrons in terms of their spatial arrangement and energy levels. This information is crucial for understanding our materials stability, reactivity, and biological activity.

4. Conclusion

In this contribution, N-acyl amino acids **P1** and **P2** synthesis has been achieved. **P1** and **P2** were produced in a one-step process with high to outstanding yields, and their structures were investigated via NMR (^{1}H and ^{13}C), UV–Vis, FT–IR, and LC–MS analysis and were ascertained for their *in vitro* antimicrobial potential against Gram–positive bacteria: *Bacillus subtilis subsp*. *Spizizenii*ATCC 6633. The results showed that: (I) The PBE0 and BVP86 functionals give the high μ value in comparison with that calculated at ωB97X −D, B3LYP, and M06 −2X levels. (II) (III) The predictions show a progressive augmentation in ⟨α⟩ when passing from the B3LYP, M06-2X, and ωB97X −D to PBE0 and BVP86 levels with a negligible difference between ⟨α⟩ and $\Delta\alpha$ for the BVP86 and PBE0. (IV) A direct correlation has been obtained between the β_{HRS} and $\beta_{//}$, and opposite variations were obtained between β_{tot} and E_g. (V) High β_{HRS} has been obtained at lower E_g. (VI) A satisfactory agreement has been achieved between the computed E_g values and the corresponding experimental values. The β values of our N-acyl glycine derivatives are moderate, and according to Wergifosse *et al.* [33] and Alparone [34], the formation of oligomers containing these N-acyl glycine units might achieve large β responses. Another method to enhance β of these glycines consists in introducing strong acceptor groups like the nitro NO_2, as this was carried out by Jassem *et al.* [104] in the case of glycine-4-nitro benzaldehyde.

CRediT authorship contribution statement

Nour El Houda Nourai: Visualization, Methodology, Investigation, Funding acquisition. **Fatiha Sebih:** Resources. **Djebar Hadji:** Writing – original draft, Writing – review & editing, Validation, Investigation. **Fatima Zohra Allal:** Resources. **Soulef Dib:** Resources, Data curation. **Nadia Kambouche:** Software, Resources. **Valérie Rolland:** Validation, Methodology. **Salima Bellahouel-Benzine:** Validation, Supervision, Project administration.

Declaration of competing interest

The authors declare that they have no known competing financial interests or personal relationships that could have appeared to influence the work reported in this paper.

Data availability

No data was used for the research described in the article.

Acknowledgements

This research was supported by the Algerian Ministry of Higher Education and Scientific Research as well as the directorate general for scientific research and technological development. Authors thank Dr. T. Bensafi for his English review.

Appendix A. Supplementary data

Supplementary data to this article can be found online at https://doi.org/10.1016/j.molliq.2024.124260.

References

[1] B. Tan, Y.W. Yu, M.F. Monn, H.V. Hughes, D.K. O'Dell, J.M. Walker, Targeted lipidomics approach for endogenous N-acyl amino acids in rat brain tissue, J. Chromatogr. B 877 (2009) 2890–2894, https://doi.org/10.1016/j.jchromb.2009.01.002.
[2] E. Börnstein, Ueber die Oxydation des p-Toluidins, Berichte Der Dtsch. Chem. Gesellschaft. 34 (1901) 1274–1284, https://doi.org/10.1002/cber.190103401209.
[3] E. Baumann, Ueber eine einfache methode der darstellung von benzoësäureäthern, Berichte Der Dtsch. Chem. Gesellschaft. 19 (1886) 3218–3222, https://doi.org/10.1002/cber.188601902348.
[4] C. Liu, Y. Wang, C. Chai, S. Ullah, G. Zhang, B. Xu, H. Liu, L. Zhao, Interfacial activities and aggregation behaviors of N-acyl amino acid surfactants derived from vegetable oils, Colloids Surfaces A Physicochem. Eng. Asp. 559 (2018) 54–59, https://doi.org/10.1016/j.colsurfa.2018.09.042.
[5] J.T. Kim, S.M. Terrell, V.L. Li, W. Wei, C.R. Fischer, J.Z. Long, Cooperative enzymatic control of N-acyl amino acids by PM20D1 and FAAH, Elife 9 (2020) 1–18, https://doi.org/10.7554/eLife.55211.
[6] N. Battista, M. Bari, T. Bisogno, *N*-Acyl Amino Acids: Metabolism molecular targets, and role in biological processes, Biomolecules 9 (2019) 822, https://doi.org/10.3390/biom9120822.
[7] S. Baraghithy, R. Smoum, A. Drori, R. Hadar, A. Gammal, S. Hirsch, M. Attar-Namdar, A. Nemirovski, Y. Gabet, Y. Langer, Y. Pollak, C.P. Schaaf, M.E. Rech, V. Gross-Tsur, I. Bab, R. Mechoulam, J. Tam, Magel2 Modulates Bone Remodeling and Mass in Prader-Willi Syndrome by Affecting Oleoyl Serine Levels and Activity, J. Bone Miner. Res. 34 (2019) 93–105, https://doi.org/10.1002/jbmr.3591.
[8] S.H. Burstein, N-acyl amino acids (Elmiric Acids): Endogenous signaling molecules with therapeutic potential, Mol. Pharmacol. 93 (2018) 228–238, https://doi.org/10.1124/mol.117.110841.
[9] S. Arul Prakash, R.K. Kamlekar, Function and therapeutic potential of N-acyl amino acids, Chem. Phys. Lipids 239 (2021) 105114, https://doi.org/10.1016/j.chemphyslip.2021.105114.
[10] F. Piscitelli, F. Guida, L. Luongo, F.A. Iannotti, S. Boccella, R. Verde, A. Lauritano, R. Imperatore, R. Smoum, L. Cristino, A.H. Lichtman, L.A. Parker, R. Mechoulam, S. Maione, V. Di Marzo, Protective Effects of N-oleoylglycine in a mouse model of mild traumatic brain injury, ACS Chem. Neurosci. 11 (2020) 1117–1128, https://doi.org/10.1021/acschemneuro.9b00633.
[11] H.-B. Li, T. Yang, E.M. Richards, C.J. Pepine, M.K. Raizada, Maternal treatment with captopril persistently alters gut-brain communication and attenuates hypertension of male offspring, Hypertension 75 (2020) 1315–1324, https://doi.org/10.1161/HYPERTENSIONAHA.120.14736.
[12] I.P. Singh, S.K. Jain, A. Kaur, S. Singh, R. Kumar, P. Garg, S.S. Sharma, S.K. Arora, Synthesis and antileishmanial activity of piperoyl-amino acid conjugates, Eur. J. Med. Chem. 45 (2010) 3439–3445, https://doi.org/10.1016/j.ejmech.2010.04.033.
[13] M. Connor, C.W. Vaughan, R.J. Vandenberg, N-acyl amino acids and N-acyl neurotransmitter conjugates: neuromodulators and probes for new drug targets, Br. J. Pharmacol. 160 (2010) 1857–1871, https://doi.org/10.1111/j.1476-5381.2010.00862.x.
[14] L.-C. Yang, H. Deng, H. Renata, Recent progress and developments in chemoenzymatic and biocatalytic dynamic kinetic resolution, Org. Process Res. Dev. 26 (2022) 1925–1943, https://doi.org/10.1021/acs.oprd.1c00463.
[15] A. Sivasamy, M. Krishnaveni, P.G. Rao, Preparation, characterization, and surface and biological properties of N -stearoyl amino acids, J. Am. Oil Chem. Soc. 78 (2001) 897–902, https://doi.org/10.1007/s11746-001-0361-5.

[16] M. Antoszczak, M. Sobusiak, E. Maj, J. Wietrzyk, A. Huczyński, Synthesis and antiproliferative activity of new bioconjugates of Salinomycin with amino acid esters, Bioorg. Med. Chem. Lett. 25 (2015) 3511–3514, https://doi.org/10.1016/j.bmcl.2015.06.086.

[17] L. Calzetta, M.G. Matera, P. Rogliani, M. Cazzola, Multifaceted activity of N-acetyl-l-cysteine in chronic obstructive pulmonary disease, Expert Rev. Respir. Med. 12 (2018) 693–708, https://doi.org/10.1080/17476348.2018.1495562.

[18] P. Koźmiński, P.K. Halik, R. Chesori, E. Gniazdowska, Overview of dual-acting drug methotrexate in different neurological diseases, autoimmune pathologies and cancers, Int. J. Mol. Sci. 21 (2020) 3483, https://doi.org/10.3390/ijms21103483.

[19] P. Sharma, S. Singh, T.I. Siddiqui, V.S. Singh, B. Kundu, P. Prathipati, A. K. Saxena, D.K. Dikshit, L. Rastogi, C. Dixit, M.B. Gupta, G.K. Patnaik, M. Dikshit, α-Amino acid derivatives as proton pump inhibitors and potent anti-ulcer agents, Eur. J. Med. Chem. 42 (2007) 386–393, https://doi.org/10.1016/j.ejmech.2006.08.016.

[20] S.N. Mostyn, T. Rawling, S. Mohammadi, S. Shimmon, Z.J. Frangos, S. Sarker, A. Yousuf, I. Vetter, R.M. Ryan, M.J. Christie, R.J. Vandenberg, Development of an N-Acyl amino acid that selectively inhibits the glycine transporter 2 to produce analgesia in a rat model of chronic pain, J. Med. Chem. 62 (2019) 2466–2484, https://doi.org/10.1021/acs.jmedchem.8b01775.

[21] M.-K. Bill, S. Brinkmann, M. Oberpaul, M.A. Patras, B. Leis, M. Marner, M.-P. Maitre, P.E. Hammann, A. Vilcinskas, S.M.M. Schuler, T.F. Schäberle, Novel glycerophospholipid, lipo- and N-acyl amino acids from bacteroidetes: Isolation, structure elucidation and bioactivity, Molecules 26 (2021) 5195, https://doi.org/10.3390/molecules26175195.

[22] G. Sathi, V.R. Gujrati, C. Nath, J.C. Agarwal, K.P. Bhargava, K. Shanker, Synthesis and pharmacological evaluation of new ethyl esters of N-Acyl amino acids as CNS agents, Arch. Pharm. 315 (1982) 603–609, https://doi.org/10.1002/ardp.19823150707.

[23] Z. Chen, P. Zhang, Y. Liu, A. Mekkaoui, C. Wang, L. Zhao, B. Xu, Interfacial rheological behavior of N-acyl amino acid surfactants derived from vegetable oils, Colloids Surf. a: Physicochem, Eng. Asp. 592 (2020) 124600, https://doi.org/10.1016/j.colsurfa.2020.124600.

[24] C.-M. Lee, S.-Y. Kim, S.-H. Yoon, J.-B. Kim, Y.-S. Yeo, J.-S. Sim, B.-S. Hahn, D.-G. Kim, Characterization of a novel antibacterial N-acyl amino acid synthase from soil metagenome, J. Biotechnol. 294 (2019) 19–25, https://doi.org/10.1016/j.jbiotec.2019.01.017.

[25] P. Georgel, K. Crozat, X. Lauth, E. Makrantonaki, H. Seltmann, S. Sovath, K. Hoebe, X. Du, S. Rutschmann, Z. Jiang, T. Bigby, V. Nizet, C.C. Zouboulis, B. Beutler, A toll-like receptor 2-responsive lipid effector pathway protects mammals against skin infections with gram-positive bacteria, Infect. Immun. 73 (2005) 4512–4521, https://doi.org/10.1128/IAI.73.8.4512-4521.2005.

[26] Y. Gao, I.G. Shabalina, G.R.F. Braz, B. Cannon, G. Yang, J. Nedergaard, Establishing the potency of N-acyl amino acids versus conventional fatty acids as thermogenic uncouplers in cells and mitochondria from different tissues, Biochim. Biophys. Acta – Bioenerg. 1863 (2022) 148542, https://doi.org/10.1016/j.bbabio.2022.148542.

[27] M.P. Joshi, A. Uday, S. Rajamani, Elucidating N-acyl amino acids as a model protoamphiphilic system, Commun. Chem. 5 (2022) 147, https://doi.org/10.1038/s42004-022-00762-9.

[28] G.-J. Cheng, Y.-F. Yang, P. Liu, P. Chen, T.-Y. Sun, G. Li, X. Zhang, K.N. Houk, J.-Q. Yu, Y.-D. Wu, Role of N-acyl amino acid ligands in Pd(II)-catalyzed remote C-H activation of tethered arenes, J. Am. Chem. Soc. 136 (2014) 894–897, https://doi.org/10.1021/ja411683n.

[29] S.E. Kaskah, G. Ehrenhaft, J. Gollnick, C.B. Fischer, Concentration and coating time effects of N -acyl sarcosine derivatives for corrosion protection of low-carbon steel CR4 in salt water – defining the window of application, Corros. Eng. Sci. Technol. 54 (2019) 216–224, https://doi.org/10.1080/1478422X.2018.1564984.

[30] N. Günay, Ö. Tamer, D. Avcı, E. Tarcan, Y. Atalay, Molecular modelling, spectroscopic characterization and nonlinear optical analysis on N-Acetyl-DL-methionine, Rev. Mex. Física. 66 (2020) 749–760, https://doi.org/10.31349/RevMexFis.66.749.

[31] N. Farhan, A. Rageh Al-Maleki, S. Ataei, N. Muhamad Sarih, R. Yahya, Synthesis, DFT study, theoretical and experimental spectroscopy of fatty amides based on extra-virgin olive oil and their antibacterial activity, Bioorg. Chem. 135 (2023) 106511, https://doi.org/10.1016/j.bioorg.2023.106511.

[32] A. Salinas-Torres, H. Rojas, J.J. Martínez, D. Becerra, J.-C. Castillo, Synthesis, Characterization, and DFT Studies of N-(3,5-Bis(trifluoromethyl)benzyl) stearamide, Molbank. 2021 (2021) M1215, https://doi.org/10.3390/M1215.

[33] M. de Wergifosse, J. de Ruyck, B. Champagne, How the second-order nonlinear optical response of the collagen triple helix appears: A theoretical investigation, J. Phys. Chem. C 118 (2014) 8595–8602, https://doi.org/10.1021/jp501602a.

[34] A. Alparone, Evolution of electric dipole (hyper)polarizabilities of β-strand polyglycine single chains: An ab initio and dft theoretical study, J. Phys. Chem. A 117 (2013) 5184–5194, https://doi.org/10.1021/jp403155q.

[35] R.A. Timothy, H. Louis, E.A. Adindu, T.E. Gber, E.C. Agwamba, O.E. Offiong, A. M.S. Pembere, Elucidation of collagen amino acid interactions with metals (B, Ni) encapsulated graphene/PEDOT material: Insight from DFT calculations and MD simulation, J. Mol. Liq. 390 (2023) 122950, https://doi.org/10.1016/j.molliq.2023.122950.

[36] V. Srivastava, J. Haque, C. Verma, P. Singh, H. Lgaz, R. Salghi, M.A. Quraishi, Amino acid based imidazolium zwitterions as novel and green corrosion inhibitors for mild steel: Experimental, DFT and MD studies, J. Mol. Liq. 244 (2017) 340–352, https://doi.org/10.1016/j.molliq.2017.08.049.

[37] D. Hadji, A. Rahmouni, Theoretical study of nonlinear optical properties of some azoic dyes, Mediterr. J. Chem. 4 (2015) 185–192, https://doi.org/10.13171/mjc.4.4.2015.15.07.22.50/hadji.

[38] D. Hadji, A. Rahmouni, D. Hammoutène, O. Zekri, First theoretical study of linear and nonlinear optical properties of diphenyl ferrocenyl butene derivatives, J. Mol. Liq. 286 (2019) 110939, https://doi.org/10.1016/j.molliq.2019.110939.

[39] Y. Bekki, D. Hadji, A. Guendouzi, B. Houari, M. Elkeurti, Linear and nonlinear optical properties of anhydride derivatives: A theoretical investigation, Chem. Data Collect. 37 (2022) 100809, https://doi.org/10.1016/j.cdc.2021.100809.

[40] F.Y. Cherif, D. Hadji, N. Benhalima, Molecular structure, linear, and nonlinear optical properties of piperazine-1,4-Diium Bis 2,4,6-trinitrophenolate: A theoretical investigation, Phys. Chem. Res. 11 (2023) 33–48, https://doi.org/10.22036/pcr.2022.330752.2035.

[41] A. Merouane, A. Mostefai, D. Hadji, A. Rahmouni, M. Bouchekara, A. Ramdani, S. Taleb, Theoretical insights into the static chemical reactivity and NLO properties of some conjugated carbonyl compounds: case of 5-aminopenta-2, 4-dienal derivatives, Monatshefte Für Chemie-Chemical Mon. 151 (2020) 1095–1109, https://doi.org/10.1007/s00706-020-02653-y.

[42] D. Hadji, B. Haddad, S.A. Brandán, S.K. Panja, A. Paolone, M. Drai, D. Villemin, S. Bresson, M. Rahmouni, Synthesis, NMR, Raman, thermal and nonlinear optical properties of dicationic ionic liquids from experimental and theoretical studies, J. Mol. Struct. 1220 (2020) 128713, https://doi.org/10.1016/j.molstruc.2020.128713.

[43] A. Kenane, D. Hadji, K. Argoub, A. Yahiaoui, A. Hachemaoui, K. Toubal, A. M. Benkouider, O. Rasoga, A. Stanculescu, A. Galca, Efficient NLO materials based on poly(ortho-anisidine) and polyaniline: A quantum chemical study, J. Electron. Mater. 52 (2023) 530–539, https://doi.org/10.1007/s11664-022-10022-0.

[44] R. Gheribi, D. Hadji, R. Ghallab, M. Medjani, M. Benslimane, C. Trifa, G. Dénès, H. Merazig, Synthesis, spectroscopic characterization, crystal structure, Hirshfeld surface analysis, linear and NLO properties of new hybrid compound based on tin fluoride oxalate and organic amine molecule (C12N2H9)2[SnF2(C2O4)2]2H2O, J. Mol. Struct. 1248 (2022) 131392, https://doi.org/10.1016/j.molstruc.2021.131392.

[45] A. Benmohammed, D. Hadji, A. Guendouzi, Y. Mouchaal, A. Djafri, A. Khelil, Synthesis, characterization, linear and NLO properties of novel N-(2,4-dinitrobenzylidene)-3-chlorobenzenamine schiff base: Combined experimental and DFT calculations, J. Electron. Mater. 50 (2021) 5282–5293, https://doi.org/10.1007/s11664-021-09046-9.

[46] B. Baroudi, K. Argoub, D. Hadji, A.M. Benkouider, K. Toubal, A. Yahiaoui, A. Djafri, Synthesis and DFT calculations of linear and nonlinear optical responses of novel 2-thioxo-3-N, (4-methylphenyl) thiazolidine-4 one, J. Sulfur Chem. 41 (2020) 310–325, https://doi.org/10.1080/17415993.2020.1736073.

[47] D. Hadji, A. Rahmouni, Molecular structure, linear and nonlinear optical properties of some cyclic phosphazenes: A theoretical investigation, J. Mol. Struct. 1106 (2016) 343–351, https://doi.org/10.1016/j.molstruc.2015.10.033.

[48] W. Qiao, Z. Zheng, H. Peng, L. Shi, Synthesis and properties of three series amino acid surfactants, Tenside Surfactants Deterg. 49 (2012) 161–166, https://doi.org/10.3139/113.110179.

[49] G.N. Petrie, K.L. Wills, F. Piscitelli, R. Smoum, C.L. Limebeer, E.M. Rock, A. E. Humphrey, M. Sheppard-Perkins, A.H. Lichtman, R. Mechoulam, V. Di Marzo, L.A. Parker, Oleoyl glycine: interference with the aversive effects of acute naloxone-precipitated MWD, but not morphine reward, in male Sprague-Dawley rats, Psychopharmacology 236 (2019) 2623–2633, https://doi.org/10.1007/s00213-019-05237-9.

[50] F.Z. Abdelhadi-Bessedik, S. Dib, V. Rolland, N. Kambouche, S. Bellahouel-Benzine, Fatty acid disubstituted 1, 2, 3-triazoles: Microwave irradiated synthesis and in vitro evaluation of antimicrobial potential, Heterocycl. Lett. 9 (2019) 375–383.

[51] M.J. Frisch, G.W. Trucks, H.B. Schlegel, G.E. Scuseria, M.A. Robb, J.R. Cheeseman, G. Scalmani, V. Barone, B. Mennucci, G.A. Petersson, H. Nakatsuji, M. Caricato, X. Li, H.P. Hratchian, A.F. Izmaylov, J. Bloino, G. Zheng, J. L. Sonnenberg, M. Hada, M. Ehara, K. Toyota, R. Fukuda, J. Hasegawa, M. Ishida, T. Nakajima, Y. Honda, O. Kitao, H. Nakai, T. Vreven, J.A. Montgomery, Jr., J.E. Peralta, F. Ogliaro, M. Bearpark, J.J. Heyd, E. Brothers, K. N. Kudin, V.N. Staroverov, R. Kobayashi, J. Normand, K. Raghavachari, A. Rendell, J.C. Burant, S.S. Iyengar, J. Tomasi, M. Cossi, N. Rega, J.M. Millam, M. Klene, J.E. Knox, J.B. Cross, V. Bakken, C. Adamo, J. Jaramillo, R. Gomperts, R.E. Stratmann, O. Yazyev, A.J. Austin, R. Cammi, C. Pomelli, J.W. Ochterski, R.L. Martin, K. Morokuma, V.G. Zakrzewski, G.A. Voth, P. Salvador, J.J. Dannenberg, S. Dapprich, A.D. Daniels, O. Farkas, J.B. Foresman, J.V. Ortiz, J. Cioslowski, and D. J. Fox, Gaussian 09 (Gaussian, Inc., Wallingford CT, 2009).

[52] R.D. Dennington, T.A. Keith, J.M. Millam, GaussView5.0.8, Gaussian Inc., (2008).

[53] L.S. Kassel, The limiting high temperature rotational partition function of nonrigid molecules I. general theory. II. CH4, C2H6, C3H8, CH(CH3)3, C(CH3)4 and CH3(CH2)2CH3. III. Benzene and its eleven methyl derivatives, J. Chem. Phys. 4 (1936) 276–282, https://doi.org/10.1063/1.1749835.

[54] P.J. Stephens, F.J. Devlin, C.F. Chabalowski, M.J. Frisch, Ab initio calculation of vibrational absorption and circular dichroism spectra using density functional force fields, J. Phys. Chem. 98 (1994) 11623–11627, https://doi.org/10.1021/j100096a001.

[55] C. Adamo, M. Cossi, G. Scalmani, V. Barone, Accurate static polarizabilities by density functional theory: Assessment of the PBE0 model, Chem. Phys. Lett. 307 (1999) 265–271, https://doi.org/10.1016/S0009-2614(99)00515-1.

[56] A.D. Becke, Density-functional exchange-energy approximation with correct asymptotic behavior, Phys. Rev. a. 38 (1988) 3098–3100, https://doi.org/10.1103/PhysRevA.38.3098.

[57] S.H. Vosko, L. Wilk, M. Nusair, Accurate spin-dependent electron liquid correlation energies for local spin density calculations: a critical analysis, Can. J. Phys. 58 (1980) 1200–1211, https://doi.org/10.1139/p80-159.

[58] J.-D. Chai, M. Head-Gordon, Systematic optimization of long-range corrected hybrid density functionals, J. Chem. Phys. 128 (2008) 084106, https://doi.org/10.1063/1.2834918.

[59] Y. Zhao, D.G. Truhlar, Density functional for spectroscopy: No long-range self-interaction error, good performance for Rydberg and charge-transfer states, and better performance on average than B3LYP for ground states, J. Phys. Chem. A 110 (2006) 13126–13130, https://doi.org/10.1021/jp066479k.

[60] D. Hadji, B. Champagne, First principles investigation of the polarizability and first hyperpolarizability of anhydride derivatives, Chem. Africa. 2 (2019) 443–453, https://doi.org/10.1007/s42250-019-00060-3.

[61] R. Bersohn, P.A.O. Yoh-Han, H.L. Frisch, Double-quantum light scattering by molecules, J. Chem. Phys. 45 (1966) 3184–3198, https://doi.org/10.1063/1.1728092.

[62] R. Trastoy, T. Manso, L. Fernández-García, L. Blasco, A. Ambroa, M.L. Pérez del Molino, G. Bou, R. García-Contreras, T.K. Wood, M. Tomás, Mechanisms of bacterial tolerance and persistence in the gastrointestinal and respiratory environments, Clin. Microbiol. Rev. 31 (2018) 1–46, https://doi.org/10.1128/CMR.00023-18.

[63] P. Jelinkova, A. Mazumdar, V.P. Sur, S. Kociova, K. Dolezelikova, A.M.J. Jimenez, Z. Koudelkova, P.K. Mishra, K. Smerkova, Z. Heger, M. Vaculovicova, A. Moulick, V. Adam, Nanoparticle-drug conjugates treating bacterial infections, J. Control. Release 307 (2019) 166–185, https://doi.org/10.1016/j.jconrel.2019.06.013.

[64] E. Mühlberg, F. Umstätter, C. Domhan, T. Hertlein, K. Ohlsen, A. Krause, C. Kleist, B. Beijer, S. Zimmermann, U. Haberkorn, W. Mier, P. Uhl, Vancomycin-lipopeptide conjugates with high antimicrobial activity on vancomycin-resistant enterococci, Pharmaceuticals 13 (2020) 110, https://doi.org/10.3390/ph13060110.

[65] A.P. Desbois, V.J. Smith, Antibacterial free fatty acids: activities, mechanisms of action and biotechnological potential, Appl. Microbiol. Biotechnol. 85 (2010) 1629–1642, https://doi.org/10.1007/s00253-009-2355-3.

[66] P. Storck, F. Umstätter, S. Wohlfart, C. Domhan, C. Kleist, J. Werner, K. Brandenburg, S. Zimmermann, U. Haberkorn, W. Mier, P. Uhl, Fatty acid conjugation leads to length-dependent antimicrobial activity of a synthetic antibacterial peptide (Pep19-4LF), Antibiotics 9 (2020) 844, https://doi.org/10.3390/antibiotics9120844.

[67] M. Sreenu, R.R. Nayak, R.B.N. Prasad, Y. Poornachandra, C.G. Kumar, Surface and antimicrobial properties of N -palmitoyl amino acid-based surfactants, J. Dispers. Sci. Technol. 36 (2015) 765–771, https://doi.org/10.1080/01932691.2014.921626.

[68] S.F. Brady, J. Clardy, Long-chain N -Acyl amino acid antibiotics isolated from heterologously expressed environmental DNA, J. Am. Chem. Soc. 122 (2000) 12903–12904, https://doi.org/10.1021/ja002990u.

[69] A. Das, A. Das, B.K. Banik, Influence of dipole moments on the medicinal activities of diverse organic compounds, J. Indian Chem. Soc. 98 (2021) 100005, https://doi.org/10.1016/J.JICS.2021.100005.

[70] W. Kumler, G. Fohlen, Additions and corrections - the dipole moment and structure of urea and thiourea, J. Am. Chem. Soc. 64 (1942) 3071, https://doi.org/10.1021/ja01264a626.

[71] M. Stähelin, D.M. Burland, J.E. Rice, Solvent dependence of the second order hyperpolarizability in p-nitroaniline, Chem. Phys. Lett. 191 (1992) 245–250.

[72] A. Das, B.K. Banik, 26 - Dipole moment in medicinal research: Green and sustainable approach, in: Green Approaches in Medicinal Chemistry for Sustainable Drug Design, Elsevier, 2020, pp. 921–964, https://doi.org/10.1016/B978-0-12-817592-7.00021-6.

[73] A.L. Hickey, C.N. Rowley, Benchmarking quantum chemical methods for the calculation of molecular dipole moments and polarizabilities, J. Phys. Chem. A 118 (2014) 3678–3687, https://doi.org/10.1021/jp502475e.

[74] I. Paidarová, S.P.A. Sauer, A comparison of density functional theory and coupled cluster methods for the calculation of electric dipole polarizability gradients of methane, AIP Conference Proceedings 1504 (2012) 695–698, https://doi.org/10.1063/1.4771790.

[75] D.S. Sabirov, Polarizability of C_{60} fullerene dimer and oligomers: The unexpected enhancement and its use for rational design of fullerene-based nanostructures with adjustable properties, RSC Adv. 3 (2013) 19430–19439, https://doi.org/10.1039/c3ra42498g.

[76] K. Hatua, H.S. Das, A. Mondal, P.K. Nandi, Electronic second hyperpolarizability of alkaline earth metal chains end capped with $-NH_2$ and –CN, J. Indian Chem. Soc. 98 (2021) 100234, https://doi.org/10.1016/j.jics.2021.100234.

[77] N. Sunil Kumar, K.N.N. Prasad, S. Chandrasekhar, J. Thipperudrappa, Theoretical and photophysical investigation of biologically active fluorophore: 2-amino-6-chlorofluoren-9-one, J. Indian Chem. Soc. 99 (2022) 100767, https://doi.org/10.1016/J.JICS.2022.100767.

[78] M. Boukabene, H. Brahim, D. Hadji, A. Guendouzi, Theoretical study of geometric, optical, nonlinear optical, UV–Vis spectra and phosphorescence properties of iridium(III) complexes based on 5-nitro-2-(2′,4′-difluorophenyl) pyridyl, Theor. Chem. Acc. 139 (2020) 47, https://doi.org/10.1007/s00214-020-2560-9.

[79] D. Hadji, H. Brahim, Structural, optical and nonlinear optical properties and TD-DFT analysis of heteroleptic bis-cyclometalated iridium(III) complex containing 2-phenylpyridine and picolinate ligands, Theor. Chem. Acc. 137 (2018) 180, https://doi.org/10.1007/s00214-018-2396-8.

[80] M. Basharat, D. Hadji, Theoretical insights into the nonlinear optical properties of cyclotriphosphazene (P3N3Cl6), tris(4–hydroxyphenyl) ethane and their various inorganic–organic hybrid derivatives, J. Mater. Sci. 57 (2022) 6971–6987, https://doi.org/10.1007/s10853-022-07088-w.

[81] D. Hadji, K. Bousmaha, M. Boumediene, NLO azo compounds with sulfonamide groups: A theoretical investigation, J. Indian Chem. Soc. 100 (2023) 101062, https://doi.org/10.1016/j.jics.2023.101062.

[82] D. Hadji, A. Benmohammed, Y. Mouchaal, A. Djafri, Synthesis and characterization of novel thiosemicarbazide for nonlinear optical applications: combined experimental and theoretical study, Rev. Roum. Chim. 68 (2023) 461–469, https://doi.org/10.33224/rrch.2023.68.9.07.

[83] T. Bensafi, D. Hadji, A. Yahiaoui, K. Argoub, A. Hachemaoui, A. Kenane, B. Baroudi, K. Toubal, A. Djafri, A.M. Benkouider, Synthesis, characterization and DFT calculations of linear and NLO properties of novel (Z)-5-benzylidene-3-N(4-methylphenyl)-2-thioxothiazolidin-4-one, J. Sulfur Chem. 42 (2021) 645–663, https://doi.org/10.1080/17415993.2021.1951729.

[84] D. Hadji, Phosphates branching effect on the structure, linear and NLO properties of linear phosphazenes, Mater. Chem. Phys. 262 (2021) 124280, https://doi.org/10.1016/j.matchemphys.2021.124280.

[85] J.I. Aihara, Reduced HOMO-LUMO gap as an index of kinetic stability for polycyclic aromatic hydrocarbons, J. Phys. Chem. a. 103 (1999) 7487–7495, https://doi.org/10.1021/jp990092i.

[86] D. Seebach, Frontorbitale: Frontier Orbitals and Organic Chemical Reactions. Von I. Fleming. John Wiley & Sons, London 1976. 1. Aufl., V, 249 S., geh. § 3, 95., Nachrichten Aus Chemie, Tech. Und Lab. 25 (1977) 33–33. 10.1002/nadc.19770250113.

[87] P. Makuła, M. Pacia, W. Macyk, How to correctly determine the band gap energy of modified semiconductor photocatalysts based on UV-Vis spectra, J. Phys. Chem. Lett. 9 (2018) 6814–6817, https://doi.org/10.1021/acs.jpclett.8b02892.

[88] X. Li, S. Yu, M. Yang, C. Xu, Y. Wang, L. Chen, Electronic structure analysis of glycine oligopeptides and glycine–tryptophan oligopeptides, Physica E Low Dimens. Syst. Nanostruct. 57 (2014) 63–68, https://doi.org/10.1016/j.physe.2013.10.028.

[89] K. Fukui, Role of frontier orbitals in chemical reactions, Science 218 (1982) 747–754, https://doi.org/10.1126/science.218.4574.747.

[90] G. Venkatesh, S. Haseena, J.S. Al-Otaibi, Y.S. Mary, P. Vennila, Y. Shyma Mary, S. A.K. Azad, Observations into the reactivity, docking, DFT, and MD simulations of fludarabine and clofarabine in various solvents, J. Mol. Liq. 383 (2023) 122076, https://doi.org/10.1016/j.molliq.2023.122076.

[91] M. Muthukkumar, T. Bhuvaneswari, G. Venkatesh, C. Kamal, P. Vennila, S. Armaković, S.J. Armaković, Y. Sheena Mary, C. Yohannan, Panicker, Synthesis, characterization and computational studies of semicarbazide derivative, J. Mol. Liq. 272 (2018) 481–495, https://doi.org/10.1016/j.molliq.2018.09.123.

[92] M. Samsonowicz, E. Regulska, R. Świsłocka, A. Butarewicz, Molecular structure and microbiological activity of alkali metal 3,4-dihydroxyphenylacetates, J. Saudi Chem. Soc. 22 (2018) 896–907, https://doi.org/10.1016/j.jscs.2018.01.009.

[93] R.G. Pearson, Hard and soft acids and bases, HSAB, part 1: Fundamental principles, J. Chem. Educ. 45 (1968) 581, https://doi.org/10.1021/ed045p581.

[94] R.G. Pearson, Absolute electronegativity and hardness: applications to organic chemistry, J. Org. Chem. 54 (1989) 1423–1430, https://doi.org/10.1021/jo00267a034.

[95] R.G. Pearson, Hard and soft acids and bases, J. Am. Chem. Soc. 85 (1963) 3533–3539, https://doi.org/10.1021/ja00905a001.

[96] J. Aihara, Reduced HOMO−LUMO gap as an index of kinetic stability for polycyclic aromatic hydrocarbons, J. Phys. Chem. A 103 (1999) 7487–7495, https://doi.org/10.1021/jp990092i.

[97] P.K. Chattaraj, U. Sarkar, D.R. Roy, Electrophilicity index, Chem. Rev. 106 (2006) 2065–2091, https://doi.org/10.1021/cr040109f.

[98] R.G. Parr, L.V. Szentpály, S. Liu, Electrophilicity index, J. Am. Chem. Soc. 121 (1999) 1922–1924, https://doi.org/10.1021/ja983494x.

[99] T. Koopmans, Über die zuordnung von wellenfunktionen und eigenwerten zu den einzelnen elektronen eines atoms, Physica 1 (1934) 104–113, https://doi.org/10.1016/S0031-8914(34)90011-2.

[100] T.A. Yousef, G.M. Abu El-Reash, R.M. El Morshedy, Structural, spectral analysis and DNA studies of heterocyclic thiosemicarbazone ligand and its Cr(III), Fe(III), Co(II) Hg(II), and U(VI) complexes, J. Mol. Struct. 1045 (2013) 145–159, https://doi.org/10.1016/j.molstruc.2013.03.060.

[101] B. Yadav, R.K. Yadav, G. Srivastav, R.A. Yadav, Experimental Raman, FTIR and UV-vis spectra, DFT studies of molecular structures and barrier heights, thermodynamic functions and bioactivity of kaempferol, J. Mol. Struct. 1258 (2022) 132637, https://doi.org/10.1016/j.molstruc.2022.132637.

[102] A. Nataraj, V. Balachandran, T. Karthick, Molecular orbital studies (hardness, chemical potential, electrophilicity, and first electron excitation), vibrational investigation and theoretical NBO analysis of 2-hydroxy-5-bromobenzaldehyde by density functional method, J. Mol. Struct. 1031 (2013) 221–233, https://doi.org/10.1016/j.molstruc.2012.09.047.

[103] P. Pérez, L.R. Domingo, A. Aizman, R. Contreras, Chapter 9 The electrophilicity index in organic chemistry, Theoretical Aspects of Chemical Reactivity 19 (2007) 139–201, https://doi.org/10.1016/S1380-7323(07)80010-0.

[104] A.M. Jassem, Q.M.A. Hassan, F.A. Almashal, H.A. Sultan, A.M. Dhumad, C. A. Emshary, L.T.T. Albaaj, Spectroscopic study, theoretical calculations, and optical nonlinear properties of amino acid (glycine)-4-nitro benzaldehyde-derived Schiff base, Opt. Mater. 122 (2021) 111750, https://doi.org/10.1016/j.optmat.2021.111750.